Soft Matter

Accepted Manuscript

ROYAL SOCIETY OF CHEMISTRY

www.rsc.org/softmatter

ARTICLE TYPE www. rsc.org/xxxxxx | XXXXXXXX

The Hydrodynamics of Colloidal Gelation†

Zsigmond Varga, Gang Wang, and James Swan*

Received Xth XXXXXXXXXX 20XX, Accepted Xth XXXXXXXXX 20XX
First published on the web Xth XXXXXXXXXX 200X
DOI: 10.1039/b000000x

Colloidal gels are formed during arrested phase separation. Sub-micron, mutually attractive particles aggregate to form a system spanning network with high interfacial area, far from equilibrium. Models for microstructural evolution during colloidal gelation have often struggled to match experimental results with long standing questions regarding the role of hydrodynamic interactions. In nearly all models, these interactions are neglected entirely. In the present work, we report simulations of gelation with and without hydrodynamic interactions between the suspended particles executed in HOOMD-blue. The disparities between these simulations are striking and mirror the experimental-theoretical mismatch in the literature. The hydrodynamic simulations agree with experimental observations, however. We explore a simple model of the competing transport processes in gelation that anticipates these disparities, and conclude that hydrodynamic forces are essential. Near the gel boundary, there exists a competition between compaction of individual aggregates which suppresses gelation and coagulation of aggregates which enhances it. The time scale for compaction is mildly slowed by hydrodynamic interactions, while the time scale for coagulation is greatly accelerated. This enhancement to coagulation leads to a shift in the gel boundary to lower strengths of attraction and lower particle concentrations when compared to models that neglect hydrodynamic interactions. Away from the gel boundary, differences in the nearest neighbor distribution and fractal dimension persist within gels produced by both simulation methods. This result necessitates a fundamental rethinking of how dynamic, discrete element models for gelation kinetics are developed as well as how collective hydrodynamic interactions influence the arrest of attractive colloidal dispersions.

1 Introduction

Gelation is a common outcome of soft materials processing. In order to predict and control the material properties of gels, it is important to understand the necessary conditions for gel formation and how the gel microstructure evolves post-gelation. However, many aspects of gelation are material specific and require detailed modeling of an array of thermodynamic and transport processes. Here, we focus on particulate materials, colloids and nano-particles especially, for which gelation is ubiquitous. When desired, the applications for particulate gels are diverse. For example, particulate gels have been used to construct biodegradable artificial tissue and for scaffolds that engender cell growth in vivo[??]. They have seen applications in heterogeneous catalysis, optics, energy-harvesting and as LEDs and thermo-electrics[??]. Percolated structures are extensively studied for suitability as drug delivery implants[?] and are of interest for research on emulsions, proteins[?] and cell biology[?]. Controlled gelation is actively studied and applied in food processing, with many applications including common dairy products[?]. In industrial separation processes and during ordered self-assembly, gelation may be undesirable as well[?].

Department of Chemical Engineering, Massachusetts Institute of Technology, Cambridge MA 02139, USA.
* *Tel: +1 (617) 324-7359; E-mail: jswan@mit.edu*

Attractions between particles promote the growth of aggregates that coagulate to form a system spanning network. Because inter-particle attractions fail to produce a macroscopically condensed phase of colloids and particle motion is greatly retarded, colloidal gelation is often referred to as an arrested phase transition. The kinetics of particulate coagulation proceeding via diffusion-limited or reaction-limited aggregation are highly varied depending on the strength and range of inter-particle attraction and repulsion[?]. In many circumstances, gelation is even transient. A gel may exhibit critical slowing, but have some finite lifetime before collapsing under its own weight[?].

Although equilibrium thermodynamics dictate the stability of different phases within a dispersion of attractive colloids, the mechanism of phase separation is controlled by physical transport processes. Macroscopic phase separation typically takes on one of two forms: nucleation and growth, or spinodal decomposition[??]. The boundary between these growth regimes depends on how fluctuations arise and are dissipated within the phase separating material. In particular, past work on binary liquid-liquid phase separation has shown that structure and kinetics are sensitive to hydrodynamic flows in the phase separating material[??].

A long standing question regarding colloidal gels is the role of these hydrodynamic forces in determining the gel microstructure and gelation kinetics[?]. Figure **??** shows the ter-

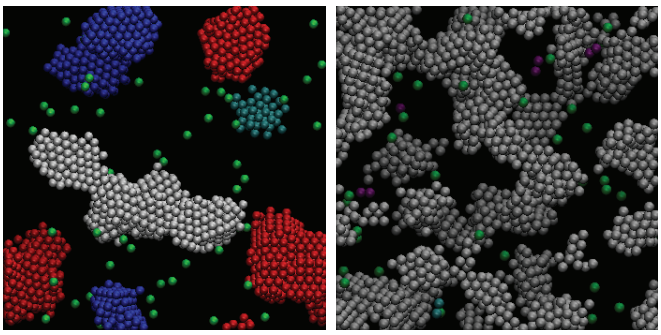

Fig. 1 Attractive particle dispersions with $\phi = 0.1$, $U_A(2a) = -5kT$, and $\delta = 0.1$ after 300 bare diffusion times (see section **??** for a definiton of these parameters). Left: without hydrodynamic interactions, right: with long-ranged hydrodynamic interactions. The right sample is gelled while the left is a dispersion of condensed droplets. Color is used to call out monomers, dimers, trimers, each other n-mer, and the system spanning cluster.

minal state of discrete element simulations using two different models for inter-particle hydrodynamic interactions under identical thermodynamic conditions. The gelation kinetics and gel microstructure depend on the dissipation mechanisms within the gel. Consequently, the rheology, coarsening and stability of colloidal gels at different ages should exhibit a sensitivity to hydrodynamic interactions between particles. These interactions are fundamentally long-ranged, which makes their mathematical description in theoretical and computational models problematic[??]. The construction of parsimonious discrete element models for colloidal gelation is important in order to understand how micro-mechanics within the arrested material give rise to macroscopic material properties that are ultimately needed for engineering applications.

For gels, whose formation is promoted by Brownian motion of particles, a number of discrete element simulations have been employed to model the microstructural evolution. The simplest simulation method, Brownian Dynamics, neglects hydrodynamic interactions among particles[?]. The results of BD simulations are gels which form at higher concentrations and attraction strengths than observed in experiments. Typically, the distributions of nearest neighbors for particles in the gel is higher than expected from experiment[?]. An alternative model, Fast Lubrication Dynamics (FLD), was used by Bybee and Higdon[?] and incorporates only lubrication interactions between nearly touching particles as a model of the inter-particle hydrodynamics. They found that there was no detectable shift in the percolation line or microstructure of the gel with respect to Brownian Dynamics and concluded that lubrication introduces only a weak shift in the gelation time scale.

Furukawa and Tanaka[?] modeled gelling colloids as viscous drops and incorporated the hydrodynamic interactions between particles via their Fluid Particle Dynamics (FPD) method. Gelation in their simulations was diffusion limited, and they observed a shift in the percolation line with respect to Brownian Dynamics simulations. This shift was consistent with experimental observations; however, no mechanism was demonstrated that could explain the shift. Cao, Cummins and Morris[?] employed Accelerated Stokesian Dynamics as a model for inter-particle hydrodynamic interactions in gels formed via reaction limited aggregation. They found a shift in the percolation line similar to Furukawa and Tanaka, and attributed the shift to the dynamics of restructuring within small aggregate clusters. How this slowing in the internal dynamics of small clusters leads to broad shifts in the percolation line was not explored.

Such detailed simulation methodologies (FLD, FPD, SD) come at great expense. All these models except Brownian Dynamics, employ 1500 particles or fewer, so that the system size is in all cases on the same order of magnitude or smaller than the pore size in the gels that form. Whether this small system size stabilizes or destabilizes nascent gels is a separate, open question. For certain, however, models which are capable of simulating larger system sizes over feasible time scales should be preferred. In the periodic geometries necessitated by computational simulation of infinite systems, the lattice dimension can have a significant impact on the hydrodynamic flows that particles generate[?]. In order to screen out system size effects in hydrodynamic interactions between particles, large system sizes are desirable when modeling kinetic phenomena such as gelation.

Four competing hydrodynamic models (BD, FLD, FPD, SD) have shown that the percolation line in colloidal gelation is sensitive to hydrodynamic interactions. The mechanism for this sensitivity is still unclear, however. BD, which neglects hydrodynamic interactions, and FLD, which includes only the short-ranged, divergent dissipative forces between particles, show higher mean contact number and percolation at higher strengths of attraction than SD and FPD simulations of similar processes. SD and FPD model both the short-ranged lubrication forces and long-ranged hydrodynamic interactions with reasonable fidelity. By elimination, long-ranged hydrodynamic interactions seem a likely candidate for the microstructural differences between models. We hypothesize that these long-ranged hydrodynammic interactions are key for colloidal gelation.

In this work, we propose a simplified hydrodynamic model that tests this hypothesis by including only long-ranged interactions between particles via the Rotne-Prager-Yamakawa tensor (RPY)[?]. RPY and BD simulations of gelation are conducted, and the same disparity in percolation and mean contact number is observed as with SD and FPD simulations of gelation. These results confirm that long-ranged hydrodynamic interactions are sufficient for establishing the gel boundary,

structure and coarsening kinetics observed in experiments and more sophisticated simulation methods. A simple macroscopic model of coagulation and compaction of particulate aggregates is used to explain why BD and FLD simulations fail to produce gels consistent with experimental evidence while SD, FPD and RPY simulations reflect experimentally observed structure and kinetics with much greater fidelity.

In short, particle aggregates continuously coagulate via diffusion – a process whose rate is strongly enhanced by long-ranged hydrodynamic interactions between the particles. At the same time, these aggregates are driven to become more compact by transitioning through various metastable, compact states – a process that is only mildly slowed by hydrodynamic interactions. When the suspension is unstable and the rate of coagulation greatly exceeds the rate of compaction, a system spanning gel results. Thus long-ranged hydrodynamic interactions are the essential physical feature of gelation, and the RPY model used herein efficiently captures this effect. Below, we briefly describe the simulation parameters before proceeding to discuss the results.

2 Materials and Methods

Simulations were performed using the HOOMD-blue suite of molecular dynamics simulation software for NVIDIA GPUs. The Brownian Dynamics simulations were run natively in HOOMD-blue, while the RPY simulations utilized a custom plug-in to HOOMD-blue built for doing large-scale hydrodynamic calculations on the GPU. This plug-in executes a version of the particle-mesh-Ewald method for modeling of Stokes flows in periodic domains[?]. Additionally, Fixman's Chebyshev polynomial approximation was used to compute the Brownian displacement at each time step in these simulations[?].

The hyper-parallelism of the GPU technologies speeds up the bottleneck in particle-mesh-Ewald methods – fast Fourier transformations – through NVIDIA's own cuFFT library. NVIDIA reports a 10x speed up when compared with many highly optimized implementations of the same algorithm. In both cases a simple GPU and multi-core CPU are compared. Similar speed ups can be achieved with CPU codes deployed over a cluster with fast inter-connects. However, the amount of hardware needed is substantially more costly than the single GPU used in the presented simulation.

The motion of monodisperse Brownian spheres over a time interval Δt can be modeled with $O(\Delta t)$ accuracy by the discrete displacement equation[?]:

$$\mathbf{x}(t+\Delta t) = \mathbf{x}(t) - \mathbf{M}\cdot\nabla U\Delta t + kT\nabla\cdot\mathbf{M}\Delta t + \Delta\mathbf{x}^B(t) \qquad (1)$$

where $\mathbf{x}(t)$ is the position of the particles at time t, kT is the thermal energy, $\mathbf{M}$ is the hydrodynamic mobility tensor, U is the inter-particle potential, and $\mathbf{x}^B(t)$ is a stochastic vector with mean: $\overline{\mathbf{x}^B(t)} = 0$ and covariance: $\overline{\mathbf{x}^B(t)\mathbf{x}^B(t)} = 2kT\mathbf{M}\Delta t$. When neglecting hydrodynamic interactions, $\mathbf{M}$ is a diagonal matrix with a single eigenvalue: $1/6\pi\eta a$, which is the Stokes mobility[?] and depends on the solvent viscosity η and the hydrodynamic radius of the particles a. This gives the particles the Stokes-Einstein diffusivity: $D = kT/6\pi\eta a$ and defines the bare diffusion time scale: $\tau_D = 6\pi\eta a^3/kT$. In Brownian Dynamics, the configuration independent mobility tensor is used as a crude model for the exact $\mathbf{M}$, which must be found at great computational expense through exact solution of the Stokes equations in the fluid phase surrounding the particles.

The exact $\mathbf{M}$ is a dense matrix which couples all the forces on the particles to their velocities and is known only for a few particle configurations such as isolated pairs of spherical particles. For any other configuration, it can be approximated with varying degrees of accuracy using SD, FLD, FPD. One approximation with high computational efficiency is the Rotne-Prager-Yamakawa tensor, which accounts only for the long-ranged hydrodynamic interactions between equal sized particles of hydrodynamic radius a. It couples the non-hydrodynamic forces exerted on particle β to the motion of particle α for an inter-particle separation $\mathbf{r}$[?]:

$$\mathbf{M}_{\alpha\beta} = \begin{cases} \frac{1}{6\pi\eta a}\mathbf{I}, & \alpha = \beta, \\ \left(1+\frac{a^2}{3}\nabla^2\right)\frac{1}{8\pi\eta r}\left(\mathbf{I}+\hat{\mathbf{r}}\hat{\mathbf{r}}\right) & \alpha\neq\beta, 2a\leq|\mathbf{r}|, \\ \frac{1}{6\pi\eta a}\left[\left(1-\frac{9r}{32a}\right)\mathbf{I}+\frac{3r}{32}\hat{\mathbf{r}}\hat{\mathbf{r}}\right] & \alpha\neq\beta, |\mathbf{r}|<2a. \end{cases} \qquad (2)$$

The RPY tensor, can be thought of as the leading order perturbation to the Stokes mobility in a Taylor series expansion of $\mathbf{M}$ about large inter-particle separations. The operation of this tensor on an arbitrary vector is efficiently evaluated using the particle-mesh-Ewald method. Even though the use of the RPY tensor in place of $\mathbf{M}$ does not fully account for many-body hydrodynamic interactions, it represents the first order improvement over Brownian dynamics and it allows introduction of far-field hydrodynamics into the numerical simulation in a controlled manner. While without lubrication forces the motion of particles during small n-mer aggregations will not be represented correctly, RPY simulations will accurately capture the hydrodynamics interactions between and relative mobility of large aggregates where there are no lubrication forces between particles present[?]. We expect this to be crucial for subsequent network formation and gelation[?].

The inter-particle potential U is evaluated pair-wise and depends only on the separation, r, between two particles. consists of two parts: an attractive contribution, $U_A(r)$, and a repulsive contribution $U_R(r)$. One common mechanism for promoting gelation is through the addition of non-absorbing polymer to a colloidal dispersion. The polymer induces inter-particle attraction through so-called depletion forces that stem from the osmotic imbalance between free polymer in so-

lution and the absence of polymer between contacting colloids. To model the depletion forces induced by non-absorbing polymer, the attractive contribution is chosen to match the Asakura-Oosawa potential[?] :

$$U_A(r) = U_A(2a)\frac{2(2a(1+\delta))^3 - 3r(2a(1+\delta))^2 + r^3}{2(2a(1+\delta))^3 - 6a(2a(1+\delta))^2 + (2a)^3}, \quad (3)$$

for $2a < r < 2a(1+\delta)$. The quantity δ is the ratio of the polymer radius of gyration to the particle radius, and $U_A(2a)$ is linearly proportional to the polymer concentration. For $\delta < 0.15$, the assumption of pair-wise additivity of attractive potentials is well founded[?] .

The repulsive contribution to the inter-particle potential is modeled here as though the particles were hard-spheres. Such a potential is easy to realize experimentally and parameter free. Using the method of Heyes and Melrose[?] , inter-particle overlaps induce a spring-like force with a magnitude sufficient to push the particles exactly back into contact over the next time step, Δt, while following the dynamics dictated by the discrete displacement equation. This potential thus depends on the mechanism for energy dissipation. In the absence of hydrodynamic interactions, the hard-core repulsion is represented by:

$$U_R(r) = \frac{3\pi\eta a}{2\Delta t}(2a - r)^2, \quad (4)$$

for $r < 2a$. For an overlapping pair of particles that interact hydrodynamically via the RPY tensor, the inter-particle potential which returns them to contact is:

$$U_R(r) = \frac{16\pi\eta a^2}{\Delta t}\left(2a\log\left(\frac{2a}{r}\right) + r - 2a\right), \quad (5)$$

for $r < 2a$. When utilized in the absence of attractions, these hard-core repulsive potentials replicate the microstructure, osmotic pressure and phase behavior of hard-sphere dispersions known from classical statistical mechanics. These potentials have the advantage of being athermal, which means they can be adapted without alteration to simulations of flowing processes.

Figure **??** plots the streamlines of the flow field generated by a point force in periodic Stokes flow. This is the principal, long-ranged flow generated by particulate motion, and as indicated in the figure, the streamlines are scale independent. In order to screen out system size effects in hydrodynamic interactions, models which are capable of simulating larger system sizes over feasible time scales should be preferred.

The RPY hydrodynamic model has several computational advantages over SD and FPD that enable rapid simulations of much larger gelling systems at the expense of accuracy. First, inclusion of only the leading order long-ranged hydrodynamic interactions allows the RPY simulation to describe hydrodynamic flows without resolving or approximating high-order

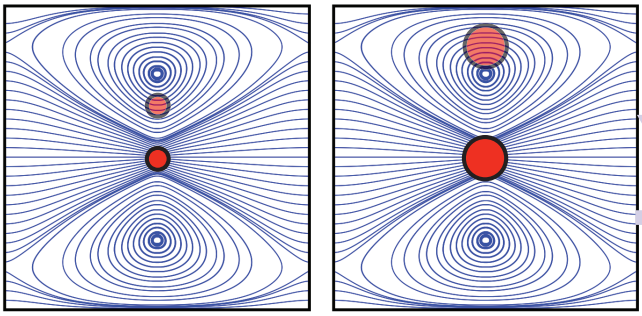

Fig. 2 The Stokes flow streamlines produced by a horizontally moving particle (solid) in a periodic domain. The particles occupies 8 times more volume in the plot on the right. The translucent particles are positioned at equivalent inter-particle separations relative to their radii, but are entrained differently by the periodic Stokes flow. The size of the periodic domain can have a significant impact on how other particles interact hydrodynamically.

contributions to the hydrodynamic scattering series. Computationally, this avoids matrix inversion which is a significant source of numerical complexity in these other methods. Second, the RPY model is easily implemented on GPUs, which enables a highly parallel execution of the model for maximal computational efficiency.

3 Results and discussion

Attractive particle dispersions were simulated with and without hydrodynamic interactions at 5 volume fractions: $\phi = 0.05, 0.1, 0.15, 0.2, 0.25$. The strength of the inter-particle attraction, $U_A(2a)$, was varied relative to the thermal energy kT, and the range of the inter-particle attraction was restricted to inter-particle separations smaller than $2a(1+\delta)$, with $\delta = 0.1$. Simulations were run with a time step $\Delta t = 10^{-4}\tau_D$ for an initial $100\tau_D$ without inter-particle attractions to ensure thermal equilibration, and for subsequent $300\tau_D$ with the attraction turned on.

The number of particles used in the simulations was $N = 8000$ with hydrodynamic interactions and $N = 64000$ without. Simulations were run with $N = 2000$ and $N = 6000$ for each of these two cases as well. For clarity, we only report data for the largest simulations. In figure **??** the structure factors,

$$S(q) = \left\langle \frac{1}{N}\sum_{j,k=1}^{N} exp\left(i\mathbf{q}\cdot(\mathbf{x}_j - \mathbf{x}_k)\right)\right\rangle, \quad (6)$$

for identical conditions but at different system sizes obtained with both RPY and BD are shown. $S(q)$, that quantifies spatial correlations between particle positions over distances $\approx 2\pi/q$, is essentially independent of N, with the peak at $q \approx 4$ quantifying the contribution of bonded particles. At the analyzed

conditions the system is found to be dynamically percolated, and as such the peak in $S(q)$ at small wave vectors ($q \to 0$) is indicative of system spanning network formation and suggests that no systematic system size effects are present. However, at the smallest values of q, differences in the structure factor as a function of system size emerge, since naturally the spatial correlations on the length scale of the simulation box are dependent on the box size and hence the number of particles N at fixed ϕ. While there is no guarantee that the sizes studied are sufficient to establish system size independence, to the authors' knowledge $N = 8000$ represents the largest simulated systems accounting for far-field hydrodynamics.

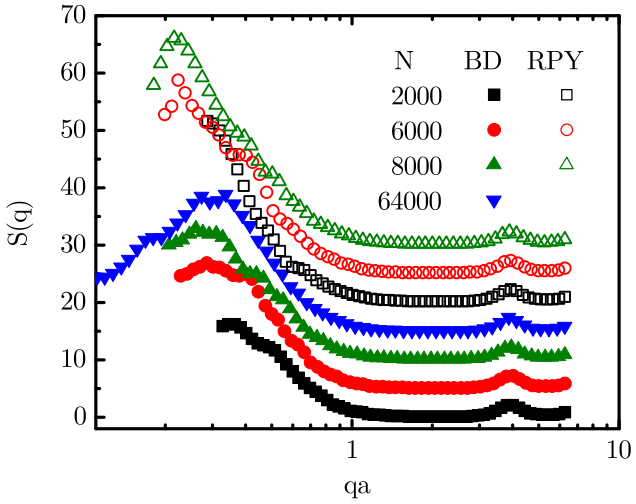

Fig. 3 Static structure factor at $U_A(2a) = -6kT$, $\delta = 0.1$, $\phi = 0.1$ and $t = 300\tau_D$ for BD and RPY simulations at three different system sizes: $N = 2000, 6000$, 8000 and 64000(BD only). For clarity, a constant vertical offset of 5 units was added between structure factors (except for BD $N = 2000$). Sample to sample fluctuations over ten(BD) or five(RPY) independently generated instances correspond to deviations of $\pm 3\%$ - error bars not shown.

Under many equivalent conditions, the RPY simulation results in a gelled dispersion that has pore sizes significantly smaller than the periodic simulation domain while the BD simulation results in a phase of dispersed, highly crystalline domains (see fig. **??**). Characterization of the gel state proceeds by identifying all bonded particles pairs that are within the range of the attractive well and constructing an adjacency matrix that is searched for clusters. The largest cluster is system spanning and dynamically percolated if on including the simulation's periodic images, the new adjacency matrix contains a path connecting the cluster to its periodic images in all three dimensions. Above the percolation threshold, almost all particles (more than 99%) belong to a persistent, connected network of particles spanning the whole system.

A phase diagram for the dispersions determined from BD and RPY simulations is depicted in figure **??**. The dashed black line corresponds to the fluid-crystal binodal given by scaled particle theory[?]. The RPY simulations exhibit gelation at lower strengths of attraction than those where hydrodynamic interactions were neglected. The lower threshold resides entirely within the fluid-crystal binodal. The minimal percolation point to within $0.1kT$ was determined in each case over three independently generated samples for both the BD and RPY models and is indicated on the phase diagram by the solid and dashed blue curves, respectively. The gap between the percolation thresholds is roughly $1kT$ at all but the lowest volume fraction studied. At $\phi = 0.05$ no percolation is observed for BD simulations, while for RPY simulations gelation occurs for attractions $-U_A(2a) \geq 6kT$. As simulations at such low volume fractions are quite slow, the precise location of the RPY percolation boundary is difficult to identify. For Brownian Dynamics simulations that failed to gel, simulations were run an additional 10^4 bare diffusion times to confirm that no percolation occurs.

These simulations are particularly interesting because the conditions correspond almost exactly to the seminal experimental work with depletion gels by Poon and co-workers[?]. In their work, depletion attraction strengths near $-4.0kT$ produced gels from suspensions with particle volume fractions between 5% and 20%. The ratio of polymer radius of gyration to particle radius was estimated to be 0.08, and the particles were prepared such that in the absence of polymer they exhibited purely hard-sphere characteristics. Their observation of the formation of a percolated network is consistent with the RPY simulations. BD simulations fail to replicate this observed non-equilibrium phase behavior. Accounting for far-field hydrodynamic interactions through the RPY tensor yields an improved agreement with experiments. In BD far higher attraction strengths and volume fractions are needed to produce a gel when compared with experiments, and a broad set of attraction strengths yield complete phase separation into small crystal nuclei instead of gelation.

This observation is corroborated by the contact number distributions shown in figure **??**. For suspensions with 10%, 15% and 20% particles by volume and $U_A(2a) = -5kT$ and $-7kT$, the terminal contact number distribution in BD and RPY simulations was determined. This measure gives the probability of finding a particle having a number of neighbors with an interparticle separation smaller than $2a(1+\delta)$. For the weaker attraction, the contact number distribution from BD simulations displays a high degree of crystallinity in contrast to the RPY simulations where gelation is observed at all volume fractions. For the stronger attraction, the models show similar contact number distributions with peaks near the Maxwell iso-staticity condition, $N_c = 6$. Notably, the BD simulations exhibit many more particles with contact numbers greater than six.

Gelation occurs when the dispersed phase of a suspension

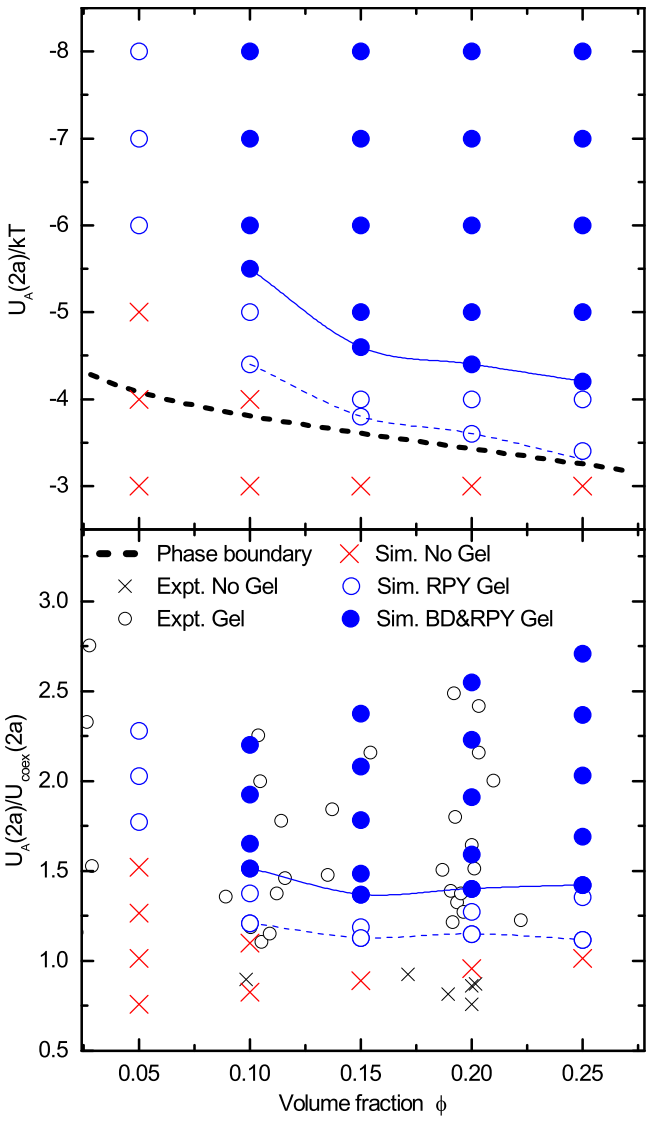

Fig. 4 Top: Phase diagram for attractive particle dispersions with $\delta = 0.1$. Non-equilibrium phases are indicated with filled symbols for simulations in the absence of hydrodynamic interactions and open symbols with hydrodynamic interactions. Bottom: Comparison of simulations with experiments from Poon and co-workers[?] . The interaction potentials are normalized by the co-existence values ($U_{coex}(2a)$) at each volume fraction ϕ. The difference between the experiments and the simulations is the polymer size ratio which was estimated to be 20% smaller, $\delta = 0.08$, in the experiment. The blue dashed and solid lines indicate the percolation boundary in RPY and BD simulations respectively.

becomes meta-stable or unstable with respect to a condensed phase. The kinetics of the transition to the condensed state on quenching from the dispersed one are controlled by two competing processes: compaction of individual aggregates which

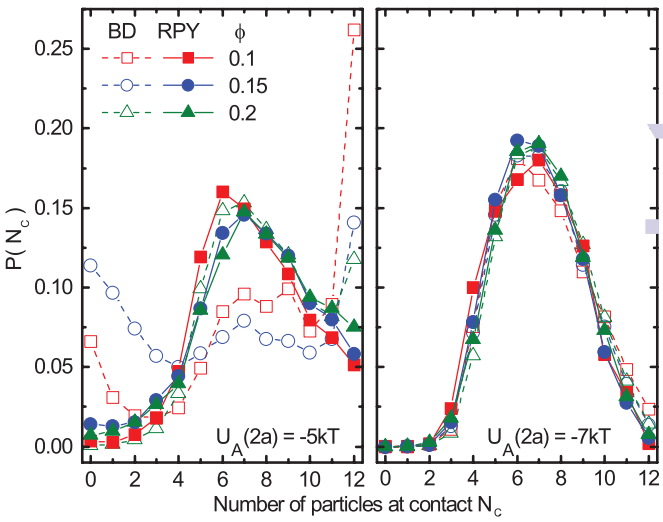

Fig. 5 Contact number distributions for attractive particle dispersions after 300 bare diffusion times with $\phi = 0.1$, 0.15 and 0.2, $\delta = 0.1$. Left: $U_A(2a) = -5kT$ and right: $U_A(2a) = -7kT$.

seeks to maximize inter-particle contacts and minimize surface energy, and coagulation of different aggregates. This is true whether the mechanism for gelation is spinodal or nucleation driven. When compaction is much faster than coagulation, the condensed phase of the suspension will tend to have minimal volume and surface area, and phase separation will proceed to completion. When compaction is much slower than coagulation, the condensed phase will be space spanning and have high surface area. If the resulting gel coarsens slowly enough, phase separation appears to arrest. The onset of gelation is observed when these two rate processes are comparable.

The rate of compaction is set by the Kramer's hopping of particles within an aggregate between different meta-stable configurations[?] . Theories for chemical kinetics evaluate transition rates from one meta-stable state to another from a properly weighted sampling of different paths through such a landscape. However, Kramer's theory for such rate processes indicates that the kinetics are dominated by the magnitude of energy barriers at suitable transition states in the landscape: ΔU. The time scale associated with the compaction process is proportional to $e^{\Delta U/kT}$, and the coefficient of proportionality has only a mild sensitivity to the energy dissipation mechanism: hydrodynamic interactions between the particles[?] . The height of the energy barriers resisting compaction are difficult to estimate since these barriers are highly configuration dependent. In general these should be proportional to the strength of attraction $U_A(2a)$, and the time scale for compaction should increase exponentially as attractions between particles grow stronger due to growth of these energy barriers.

There is an additional rate process to consider: the break-up

of aggregates. Like the time scale for compaction, this is also set by a Kramers escape time, τ_K. For a particle bound by depletion interactions this time scale is: $\tau_K/\tau_D = \delta^2 e^{N_b|U(2a)|/kT}$ where N_b is the number of bonds between particles that would need to be broken for the particle to escape. This ratio is more than four for $N_b \geq 2$ and $|U(2a)/kT| \geq 3$ and grows exponentially with respect to both. Therefore, in the domain of interest, break-up of all but the smallest aggregates occurs at a vanishingly small rate.

The mean-field Smoluchowski coagulation equation governing the time rate of change of the number density of aggregates containing i particles, $n_i(t)$,[?] depends on the coagulation rate of other diffusing aggregates:

$$\frac{\partial n_i(t)}{\partial t} = \frac{1}{2}\sum_{j=1}^{i-1} K(i-j,j)n_{i-j}(t)n_j(t) - \sum_{j=1}^{\infty} K(i,j)n_i(t)n_j(t). \quad (7)$$

$K(i,j)$ is the so-called coagulation kernel that describes the rate at which aggregates containing i and j particles collide and cohere within the suspension, and can be written as:

$$K(i,j) = 4\pi(a_i + a_j)D_{ij}/W_{ij}, \quad (8)$$

where, a_i is the collision radius of an aggregate with i particles, D_{ij} is the relative rate of bare diffusion between aggregates of size i and j, and W_{ij} is the collision efficiency:

$$W_{ij} = (a_i + a_j)\int_{a_i+a_j}^{\infty} \frac{D_{ij}e^{U_A(r)}}{r^2 D_{ij}(r)}\,dr. \quad (9)$$

As $r \to \infty$, $D_{ij}(r) \to D_{ij}$. $D_{ij}(r)$ reflects the reduction in relative diffusivity due to hydrodynamic interactions between two aggregates. The coagulation kernel regulates the rate at which aggregates grow in solution. It is an essential component of the Smoluchowski equation describing conservation of the aggregate size distribution within the suspension. The effect of hydrodynamic interactions on the coagulation kernel is twofold: through the relative diffusivity and through the collision efficiency.

The effect of inter-particle hydrodynamic interactions on the relative diffusivity is easily understood by considering the two limiting simulation cases: Brownian Dynamics in which hydrodynamic interactions are neglected, and the RPY simulations in which long-ranged interactions are modeled with high fidelity. When neglecting hydrodynamic interactions, an aggregate of i particles moving with velocity $\mathbf{U}$ feels a drag force resisting its motion: $\mathbf{F} = -6\pi\eta i a\mathbf{U}$. By the fluctuation dissipation theorem[?], the relative rate of diffusion of two such aggregates is:

$$D_{ij} = \frac{kT}{6\pi\eta a}\left(\frac{1}{i} + \frac{1}{j}\right). \quad (10)$$

That is, the relative diffusivity is proportional to the sum of the reciprocals of the numbers of particles within the aggregates. This resembles Rouse diffusion in polymer mechanics[?]. If the hydrodynamic model were extended to support inclusion of only near-field hydrodynamic interactions between particles in the aggregates – as with FLD – the same scaling of the aggregate diffusivity will result. Diffusion of aggregates in simulations where hydrodynamic lubrication is the only mechanism for energy dissipation is identical to diffusion in those which neglect hydrodynamic interactions entirely.

In contrast, an aggregate moving with velocity $\mathbf{U}$ and made of i particles, which interact via long-ranged hydrodynamic interactions, feels a drag force: $\mathbf{F} = -6\pi\eta l i^{1/d_f}\mathbf{U}$[?]. The quantity d_f is the fractal dimension of the aggregate, and l is the shape factor or lacunarity of the aggregate, which is proportional to the particle size a. In this case, the relative rate of diffusion of two aggregates is:

$$D_{ij} = \frac{kT}{6\pi\eta l}\left(\frac{1}{i^{1/d_f}} + \frac{1}{j^{1/d_f}}\right). \quad (11)$$

Although such a scaling relation cannot be precise for small aggregates, its form suggests the correct physics – that the rate of diffusion scales with the inverse of the physical size of the aggregate. Since $d_f \geq 1$ for a physical aggregate, relative diffusion in models that include long-ranged hydrodynamic interactions is substantially faster than in those that neglect them. When neglecting hydrodynamic interactions, particles in an aggregate behave as point sources of resistance as though the aggregate had a fractal dimension of just 1. Long-ranged hydrodynamic interactions among particles in an aggregate lead to screening which enhances the rate of aggregate motion.

Recall that the rate of compaction is relatively insensitive to the dissipation mechanism. Therefore, large and highly immobile aggregates modeled in the absence of hydrodynamic interactions will tend to show significant compaction relative to coagulation. This fully explains the observed shift in the percolation line and contact number distributions when comparing the two methodologies. Without hydrodynamic interactions, a suspension requires deeper quenches or higher particle densities to form large aggregates that percolate and kinetically arrest.

In contrast, long-range hydrodynamic interactions lead to aggregates that are highly mobile. As these aggregates become more compact, their fractal dimension increases and they become more mobile still. This feedback promotes coagulation and drives formation of a system spanning network at conditions consistent with experimental observations[??]. The time scale for coagulation is highly sensitive to the long-range hydrodynamic interactions between particles. These interactions screen the drag on individual particles leading to a relative diffusivity that scales inversely with the characteristic

length scales of the aggregates: $a_i = li^{1/d_f}$. Direct evidence of aggregate formation prior to gelation is shown in figure **??**, which depicts a time series of the growth of a gel in the presence of long-ranged hydrodynamic interactions. Percolation is preceded by the formation of many large aggregates containing roughly 20 particles on average.

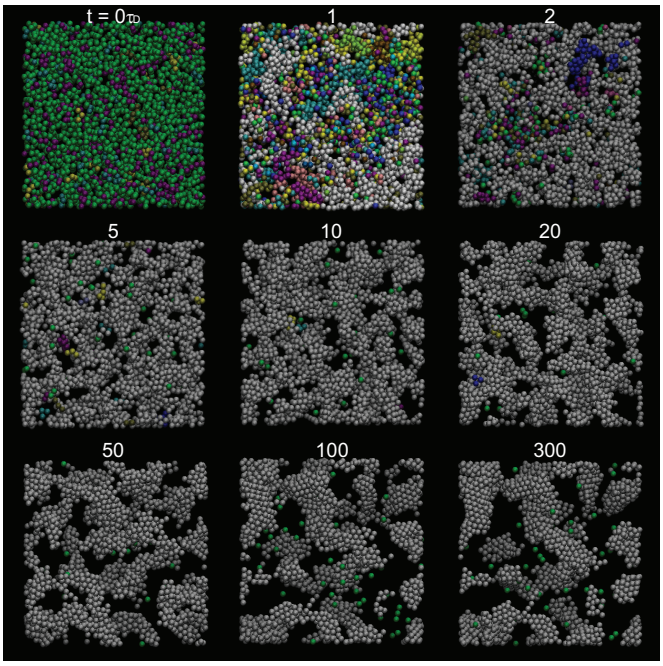

Fig. 6 Time series snapshots of a suspension with $\phi = 0.15$ and $U_A(2a) = -5kT$. The formation of aggregates containing roughly 20 particles on average precedes gelation. Color is used to call out monomers, dimers, trimers, each other n-mer, and the system spanning cluster.

Although colloidal gelation at modest volume fractions has long been viewed from the perspective of spinodal decomposition, the eventual arrest of the phase separation depends on the inherent dynamics between particles, in this case dictated by long-ranged hydrodynamic interactions. Ultimately, colloidal gelation is driven by cluster aggregation. Models for the spinodal decomposition of binary mixtures have reported similar results regarding the dynamics of phase separation[?].

The large scale structure of these same dispersions is reflected in the fractal dimension of the gels they form. At the studied concentrations and system sizes, the percolated networks are not truly fractals since self-similarity is not realized at all length scales. However, the box counting dimension of these gels for length scales large relative to the particle size and small relative to the size of the periodic box serves as a good indicator of global structure. and are in excellent agreement with the power law scaling of the total correlation function[?], i.e. $g(r) - 1 \sim r^{1-3/d_f}$. Figure **??** depicts the fractal dimension of gels observed in BD and RPY simulations as a function of volume fraction and attraction strength. A systematic but modest trend towards higher fractal dimension with increasing volume fraction is detectable. More importantly the fractal dimension of gels formed from BD is typically 15% higher than those formed from RPY simulations at the same conditions.

Even for strongly bonded, concentrated suspensions, $U_A(2a) = -8kT$ and $\phi = 0.25$ for example, where local structural differences are not observable, the large scale structure as signified by the fractal dimension differs considerably between the two simulation methods. This sensitivity of fractal dimension to hydrodynamic interactions has been noted in various simulations of diffusion limited cluster aggregation[? ? ?]. The present work indicates that collective motions of aggregated colloids bias the percolated network to lower fractal dimensions even in the case of the strong bonding and high concentration. The fractal dimension of a gel is intimately related to the gel rheology; thus, accurate models of rheological properties will exhibit great sensitivity to the pathway along which gelation proceeds[? ?].

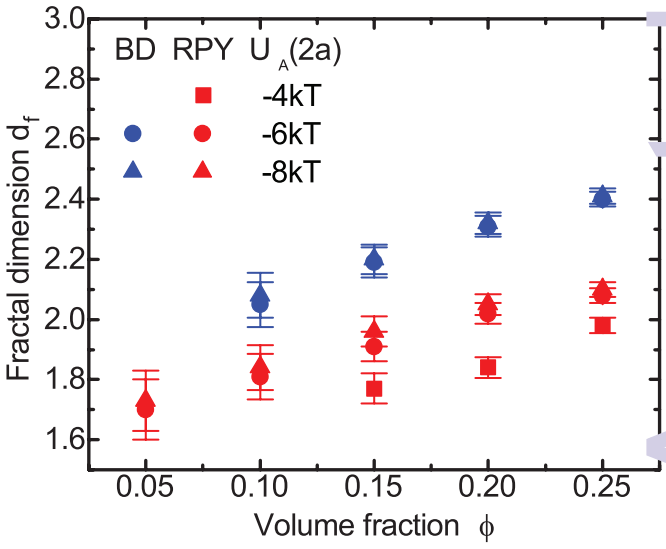

Fig. 7 The fractal dimension for gels formed in BD and RPY simulations as a function of volume fraction and strength of inter-particle attraction as determined by the box counting dimension and the power law scaling of the total correlation function. Error bars represent sample to sample fluctuations over three independently generated instances for each gel.

The second effect of hydrodynamic interactions on coagulation is through the collision efficiency. When the range of attraction between aggregates is much smaller than the mean aggregate size, the term $\exp(U_A(r)/kT)$ in equation **??** can be replaced by unity. Then, without hydrodynamic interactions, the collision efficiency is $W_{ij} = 1$. With only the leading order

long-ranged hydrodynamic interactions included, the separation dependent relative diffusivity can be written as[?]

$$D_{ij}(r) = D_{ij}\left[1 - \frac{3\beta_{ij}}{1+\beta_{ij}}\frac{a_j}{r} + \frac{\beta_{ij}(1+\beta_{ij}^2)}{1+\beta_{ij}}\left(\frac{a_j}{r}\right)^3\right], \quad (12)$$

where $\beta_{ij} = a_i/a_j$. This is an approximation which neglects contributions of shape to the relative diffusivity, but includes the leading order $1/r$, Stokeslet, and $1/r^3$, Stokes dipole, contributions for spherical aggregates of finite size. This contribution to the slowing of diffusive motion between two fractal aggregates is an underestimate but always positive, which leads to an integrable kernel for the stability ratio. With these simplifications, the collision efficiency can be fit to within 0.1% by the nearly quadratic function: $W_{ij} \approx 1.6554 - 0.6554(1-\beta_{ij})^{2.15}$, over the range $\beta_{ij} \in [0,1]$. It takes on a value of unity when $\beta_{ij} = 0$ and increases monotonically to 1.6554... when $\beta_{ij} = 1$.

Thus, long-ranged hydrodynamic interactions between aggregates introduce only a weak multiplicative dependence of the coagulation kernel on the aggregate size ratio through the collision efficiency. This effect biases the rate of aggregation to modestly favor interaction of dislike aggregates. The total coagulation kernel including hydrodynamic effects is larger than that neglecting them for all aggregate sizes when assuming $l = a$. In cases where aggregation is reaction limited, rather than diffusion limited, a repulsive inter-particle potential must be included in the collision efficiency. Then, hydrodynamic interactions can introduce significant changes to W_{ij}[?].

The effect of long-ranged hydrodynamic interactions on the rate of aggregation is depicted in figure **??**, which presents the number of n-mers with $n = 2,3,4$ as a function of time for $\phi = 0.15$, $\delta = 0.1$ and $U_A(2a)/kT = -4kT$ for both simulation methods. The n-mer distribution as a function of time from solution of Smoluchowski's coagulation equation using the diffusivities in equations **??** and **??**, assuming $W_{ij} = 1$, is presented as well. When long-ranged hydrodynamic interactions are modeled correctly, rapid gelation occurs, favoring fast growth of large clusters ($n > 4$) as small aggregates are depleted from solution. In the case that these interactions are neglected, small aggregates ($n \leq 4$) form initially and then grow slowly via monomer addition. Coagulation into larger clusters proceeds at a reduced rate and the concentration of small aggregates appears steady.

The solution of Smoluchowski's coagulation equation displays the same qualitative behavior as found for simulation of the two hydrodynamic models - a gap between the concentrations of small n-mers results from the size dependence of the aggregate diffusivity. This might be surprising given that the coagulation equation neglects compaction and break-up of aggregates entirely. However, the initial stages of gelation should be dominated by coagulation of particles in to larger

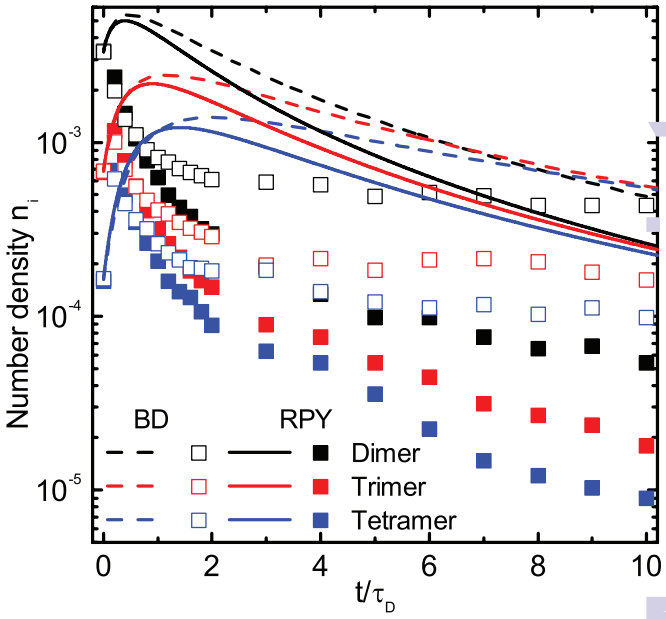

Fig. 8 The number density ($n_i = N_i 3\phi/N4\pi a^3$) of n-mers with $n = 1,2,3,4$ as a function of time for $\phi = 0.15$ and $U_A(2a) = -4kT$ in the absence of hydrodynamic interactions (open symbols) and with hydrodynamic interactions (filled symbols). The dashed and solid lines represent the solution of the Smoluchowski coagulation equation using the diffusivities in equations (**??**) and (**??**) respectively.

aggregates since compaction and break-up cannot occur without the existence of such aggregates.

For the Smoluchowski model with the BD-like diffusivity of aggregates, the concentration of small aggregates decreases mildly with time as larger clusters are slowly formed through monomer addition. With the RPY-like diffusivity of aggregates, the coagulation equation predicts a stronger decline in the number of small n-mers as they leverage their mobility t quickly coalesce into system spanning structures. As Smoluchowksi's coagulation equation describes the kinetics of binary aggregation in terms of a mean-field equation in the dilute limit ($\phi \to 0$), differences between simulation results and solutions to this equation are natural. It is possible to construct self-consistent closures to improve on these limitations and obtain more accurate predictions[??]. However, Smoluchowski's simple model is sufficient to explain the effect of hydrodynamic interactions on cluster aggregation observed in simulations.

An outstanding question that we wish to explore extensively in the future is the effect of hydrodynamic interactions on collective dynamical processes as the gel forms. The strong dependence of microscopic dynamics on the probed length scale close to gelation has been studied experimentally[?] as well as numerically[??] - however, without considering hydrodynamic

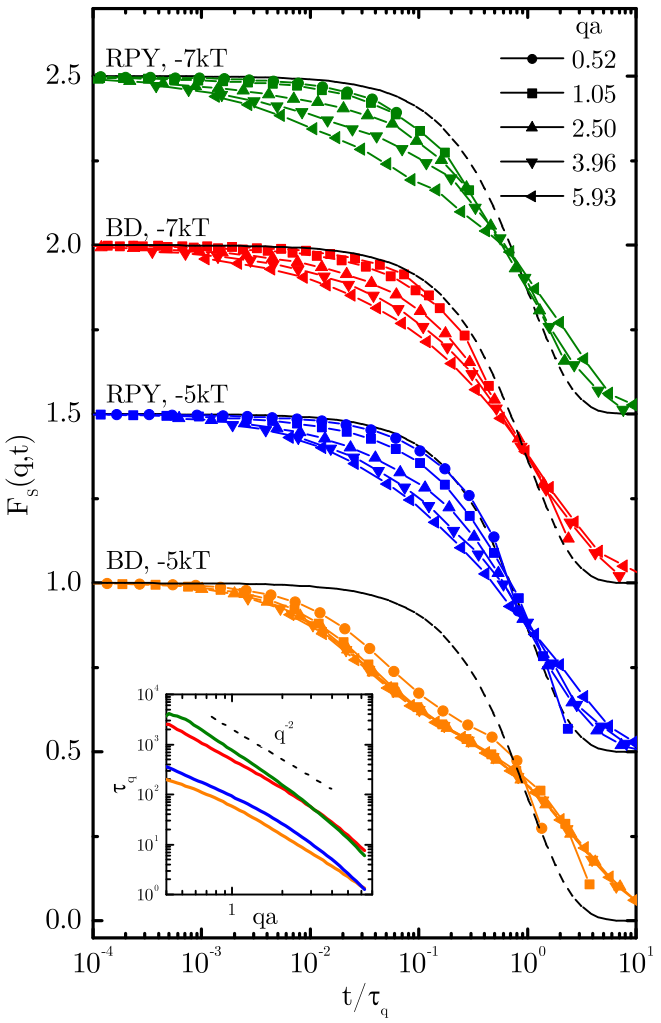

Fig. 9 The incoherent scattering function $F_s(q,t)$ for BD and RPY gels of $\phi = 0.15$, $\delta = 0.1$, $U_A(2a) = -5kT$ and $-7kT$ for selected wave vectors q at $\tau_D = 10^2$. For clarity, a constant vertical offset of 0.5 units was added between sets of $F_s(q,t)$. The dashed lines present the trivial exponential $\exp -t/\tau_q$, highlighting the compressed and stretched nature of the scattering function decay. Sample to sample fluctuations over four independently generated instances correspond to deviations of $\pm 3\%$ - error bars not shown. Inset: the characteristic relaxation time τ_q as a function of q for the four different gels - colors are the same as in the main plot.

interactions. The incoherent scattering function,

$$F(q,t) = \left\langle \frac{1}{N} \sum_{j=1}^{N} \exp\left(-i\mathbf{q}\cdot(\mathbf{x}_j(t) - \mathbf{x}_j(0))\right) \right\rangle, \qquad (13)$$

quantifies the time correlation in single particle displacements over a length scale$\approx 2\pi/q$ and a time lag t, whereas the coherent scattering function,

$$F(q,t) = \left\langle \frac{1}{NS(q)} \sum_{j,k=1}^{N} \exp\left(-i\mathbf{q}\cdot(\mathbf{x}_k(t) - \mathbf{x}_j(0))\right) \right\rangle, \qquad (14)$$

provides information on the collective dynamics of the system. The decay of the correlations from their initial plateau is indicative of network restructuring and relaxation and can be fitted by a stretched exponential $\sim \exp[-(t/\tau_q)^\beta]$, where τ_q is the structural relaxation time and β is a stretching exponent. β is strongly dependent on the shape of the distribution of relaxation modes, wider distributions leading to lower exponents.

$F_S(q,t)$ and $F(q,t)$ as a function of the normalized lag time t/τ_q for a set of wave vectors, are shown in figures **??** and **??** for two gels under different conditions obtained in BD and RPY simulations. For both simulation methods the relaxation times are found to scale as $\sim q^{-2}$ - the single-particle as well the collective modes exhibit diffusive dynamics.

Instead of a two-step decay as reported elsewhere[??], we do not observe an inertial decay at any wave-vector, presumably since our simulations are truly overdamped and inertial relaxation (the fast relaxation process) is instantaneous.

Comparing RPY and BD simulation results, it is apparent that long-range hydrodynamic interactions change gelation dynamics and generate different transport processes in the network for weak gels ($U_A(2a) = -5kT$) just above the gelation boundary. Ultimately, these differences arise from the depth of the quench into the phase separating region and is indicative that the gelation boundaries are truly different in BD and RPY, with the hydrodynamic simulations agreeing with experiments. In BD, decay of $F_S(q,t)$ is rapid, with a stretched exponent over all length scales of $\beta \approx 0.4$, signifying that the structure has not come to full arrest and the relaxation dynamic are complex and slow. Since we observe a high amount of crystallinity at these conditions (see figure **??**), such low stretching exponents may be due to both $\alpha-$ and $\beta-$relaxation occurring in the dispersion[?]. Consequently the collective modes exhibit a narrow relaxation spectrum with little long-range correlation. At the same conditions for RPY, when long-ranged hydrodynamics are considered, the gel is fully arrested and dynamics are dependent on the size of the region under analysis. For small q, $F_S(q,t)$ decays close to exponentially ($\beta \approx 1$). However, for smaller length scales, the decay of the correlations is stretched, with β decreasing linearly and approaching a value close to ~ 0.5, suggestive of a broad relaxation spectrum. The decay of $F(q,t)$ is also broadened compared to BD, hinting that dynamics are affected by the restructuring of the network and that the dispersion is characterized by strong cooperativity due to the presence of long-range hydrodynamic interactions.

In contrast, as already observed in the case of the terminal contact number distribution, strong gels far from the boundary ($U_A(2a) = -7kT$) are less sensitive and exhibit similar

dynamics. However, observable differences in the relaxation mechanisms persist both for the single-particle and collective motion.

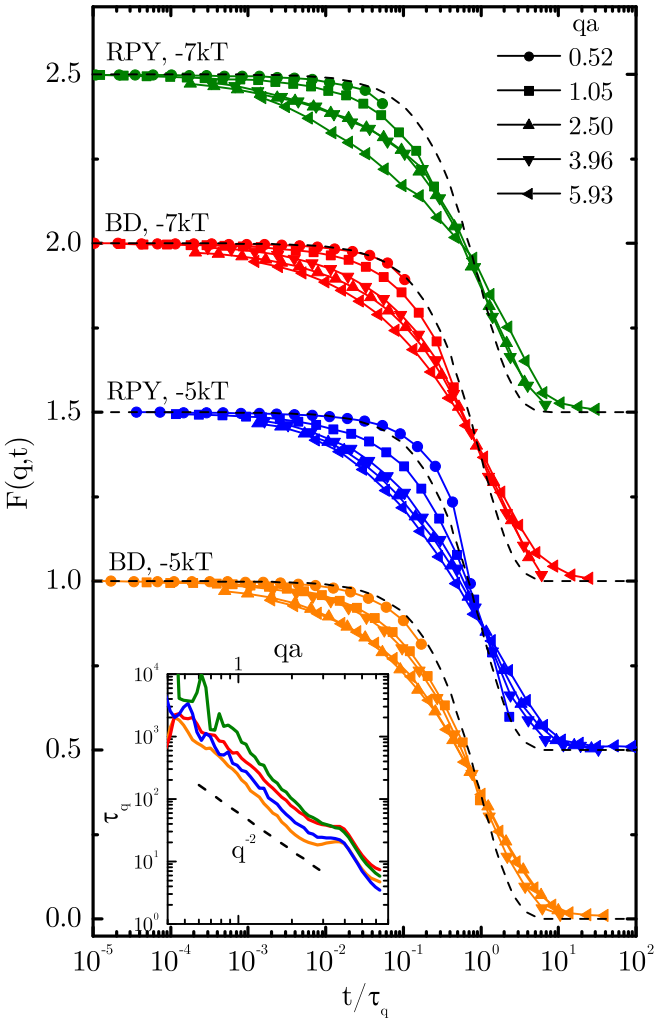

Fig. 10 The coherent scattering function $F(q,t)$ for BD and RPY gels of $\phi = 0.15$, $\delta = 0.1$, $U_A(2a) = -5kT$ and $-7kT$ for selected wave vectors q at $\tau_D = 10^2$. For clarity, a constant vertical offset of 0.5 units was added between sets of $F(q,t)$. The dashed lines present the trivial exponential $\exp -t/\tau_q$, highlighting the compressed and stretched nature of the scattering function decay. Sample to sample fluctuations over four independently generated instances correspond to deviations of $\pm 1\%$ - error bars not shown. Inset: the characteristic relaxation time τ_q as a function of q for the four different gels - colors are the same as in the main plot.

This initial analysis on the particle dynamics in the percolated system shows that the long-range correlations and particle cooperativity near the gelation boundary are sensitive to hydrodynamic interactions between colloids and hence aggregate diffusion rates. Changes in the organization and restructuring of the network due to hydrodynamic interactions also ultimately determine the terminal state of an attractive suspension and hence influence the location of the observed dynamic percolation line.

4 Conclusions

This work has demonstrated a minimal discrete element model for colloidal gelation and highlighted the critical effect that long-ranged hydrodynamic interactions have on the structure and kinetics of the gelation process. Although more sophisticated hydrodynamic models such as Stokesian Dynamics can be deployed for particulate simulations, the RPY mobility used here is sufficient to capture both the shift in the percolation line and the reduction in mean contact number seen in experiment and more complicated hydrodynamic models when compared to models that neglect inter-particle hydrodynamics.

While lubrication and intermediate-range hydrodynamic interactions have been neglected, the simulations employing RPY hydrodynamics are consistent with experimental results for depletion gels, and provide strong evidence that aggregate diffusion rates are key for determining the terminal state in a dispersion of attractive particles. Additionally, this simple model of the physical processes governing gelation is computationally efficient and easy to extend to other inter-particle potentials, larger system sizes, and dispersions deformed by different driving forces. For example, when subjecting a gel to a gravitational stress using the RPY method, the formation of a streamer driven by back-flow of the solvent through the percolated structure can be observed. Such physical effects cannot be realized in Brownian Dynamics simulations. In our opinion, the ability to extend the model to other dynamic phenomena makes the RPY approach the most parsimonious for colloidal gelation.

In future investigations, we will extend the simulation method to polydisperse suspensions and incorporate both hydrodynamic lubrication and higher order long-ranged hydrodynamic forces. Polydispersity may slow the rate of compaction and break-up of aggregates by suppressing the thermodynamic driving forces for these processes. Thus, enhancement to collective motion of aggregates may be less significant. Similarly, a comparison between the RPY simulation and rapid Stokesian Dynamics simulations may allow for discrimination of more subtle hydrodynamic effects during gelation and provide a decisive assessment of the relative importance of the various hydrodynamic forces. Certainly, rapid Stokesian Dynamics simulations will enable more accurate description of the stresses in a deforming gelation.

Acknowledgments

Support from The MIT Portugal Program is gratefully acknowledged.

References

S. V. Vinogradov, T. K. Bronich and A. V. Kabanov, *Advanced drug delivery reviews*, 2002, **54**, 135–147.

Q. Wang, L. Wang, M. S. Detamore and C. Berkland, *Advanced Materials*, 2008, **20**, 236–239.

N. Gaponik, A.-K. Herrmann and A. Eychmuller, *The Journal of Physical Chemistry Letters*, 2011, **3**, 8–17.

L. Chen, B. Wei, X. Zhang and C. Li, *Small*, 2013, **9**, 2331–2340.

C. Barbe, J. Bartlett, L. Kong, K. Finnie, H. Q. Lin, M. Larkin, S. Calleja, A. Bush and G. Calleja, *Advanced materials*, 2004, **16**, 1959–1966.

S.-H. Chen, J. Rouch, F. Sciortino and P. Tartaglia, *Journal of Physics: Condensed Matter*, 1994, **6**, 10855.

R. J. Ellis and A. P. Minton, *Nature*, 2003, **425**, 27–28.

R. Mezzenga, P. Schurtenberger, A. Burbidge and M. Michel, *Nature materials*, 2005, **4**, 729–740.

P. Jiang, J. Bertone, K. Hwang and V. Colvin, *Chemistry of Materials*, 1999, **11**, 2132–2140.

E. Zaccarelli, *Journal of Physics: Condensed Matter*, 2007, **19**, 323101.

N. A. Verhaegh, D. Asnaghi, H. N. Lekkerkerker, M. Giglio and L. Cipelletti, *Physica A: Statistical Mechanics and its Applications*, 1997, **242**, 104–118.

P. R. ten Wolde and D. Frenkel, *Science*, 1997, **277**, 1975–1978.

P. G. Vekilov, *Nanoscale*, 2010, **2**, 2346–2357.

J. A. Thomson, P. Schurtenberger, G. M. Thurston and G. B. Benedek, *Proceedings of the National Academy of Sciences*, 1987, **84**, 7079–7083.

A. J. Wagner and J. Yeomans, *Physical Review Letters*, 1998, **80**, 1429.

D. Stauffer, A. Coniglio and M. Adam, *Polymer networks*, Springer, 1982, pp. 103–158.

G. Batchelor and J.-T. Green, *Journal of Fluid Mechanics*, 1972, **56**, 375–400.

J. F. Brady and G. Bossis, *Annual review of fluid mechanics*, 1988, **20**, 111–157.

M. Fixman, *The Journal of Chemical Physics*, 1978, **69**, 1527–1537.

P. J. Lu, J. C. Conrad, H. M. Wyss, A. B. Schofield and D. A. Weitz, *Physical review letters*, 2006, **96**, 028306.

M. D. Bybee, *Hydrodynamic simulations of colloidal gels: Microstructure, dynamics, and rheology*, ProQuest, 2009.

A. Furukawa and H. Tanaka, *Physical review letters*, 2010, **104**, 245702.

X. Cao, H. Cummins and J. Morris, *Journal of colloid and interface science*, 2012, **368**, 86–96.

A. Sierou and J. F. Brady, *Journal of Fluid Mechanics*, 2001, **448**, 115–146.

H. Yamakawa, *The Journal of Chemical Physics*, 1970, **53**, 436–443.

C. Beenakker, *The Journal of chemical physics*, 1986, **85**, 1581–1582.

M. Fixman, *Macromolecules*, 1986, **19**, 1204–1207.

A. J. Banchio and J. F. Brady, *The Journal of chemical physics*, 2003, **118**, 10323–10332.

A. Einstein, *Annalen der Physik*, 1905, **322**, 549–560.

P. Zuk, E. Wajnryb, K. Mizerski and P. Szymczak, *Journal of Fluid Mechanics*, 2014, **741**, R5.

J. F. Brady and G. Bossis, *Annual review of fluid mechanics*, 1988, **20**, 111–157.

H. V. Nguyen and R. C. Flagan, *Langmuir*, 1991, **7**, 1807–1814.

S. Asakura and F. Oosawa, *Journal of Polymer Science*, 1958, **33**, 183–192.

H. Lekkerkerker and R. Tuinier, *Colloids and the Depletion Interaction*, Springer, Heidelberg, 1st edn, 2011.

D. Heyes and J. Melrose, *Journal of non-newtonian fluid mechanics*, 1993, **46**, 1–28.

W. Poon, A. Pirie, M. Haw and P. Pusey, *Physica A: Statistical Mechanics and its Applications*, 1997, **235**, 110–119.

H. Kramers, *Physica*, 1940, **7**, 284–304.

R. Zwanzig, *Nonequilibrium statistical mechanics*, Oxford University Press, 2001.

M. Von Smoluchowski, *Z. Phys.*, 1916, **17**, 557–585.

S. Edwards and M. Doi, *Thetheory of polymer dynamics*, Oxford Science Publications, Oxford, UK, 1st edn, 1986.

K. Binder and D. Stauffer, *Physical Review Letters*, 1974, **33**, 1006.

A. D. Dinsmore, E. R. Weeks, V. Prasad, A. C. Levitt and D. A. Weitz, *Applied optics*, 2001, **40**, 4152–4159.

P. Sandkühler, J. Sefcik and M. Morbidelli, *Advances in colloid and interface science*, 2004, **108**, 133–143.

R. Yamamoto, K. Kim, Y. Nakayama, K. Miyazaki and D. R. Reichman, *Journal of the Physical Society of Japan*, 2008, **77**, year.

J. K. Whitmer and E. Luijten, *The Journal of Physical Chemistry B*, 2011, **115**, 7294–7300.

D. Weitz, J. Huang, M. Lin and J. Sung, *Physical review letters*, 1985, **54**, 1416.

H. E. Stanley and P. Meakin, *Nature*, 1988, **335**, 405–409.

S. Kim and S. Karrila, *Mycrohydrodynamics: Principlles and Selected Applications*, Butterworth-Heinemann, Boston, 1st edn, 1991.

L. A. Spielman, *Journal of Colloid and Interface Science*, 1970, **33**, 562–571.

M. Slemrod, *Physica D: Nonlinear Phenomena*, 1990, **46**, 351–366.

M. Yu, J. Lin and T. Chan, *Aerosol Science and Technology*, 2008, **42**, 705–713.

L. Cipelletti, S. Manley, R. Ball and D. Weitz, *Physical review letters*, 2000, **84**, 2275.

J. Colombo and E. Del Gado, *Soft matter*, 2014, **10**, 4003–4015.

R. N. Zia, B. J. Landrum and W. B. Russel, *Journal of Rheology (1978-present)*, 2014, **58**, 1121–1157.

R. J. dArjuzon, W. Frith and J. R. Melrose, *Physical Review E*, 2003, **67**, 061404.

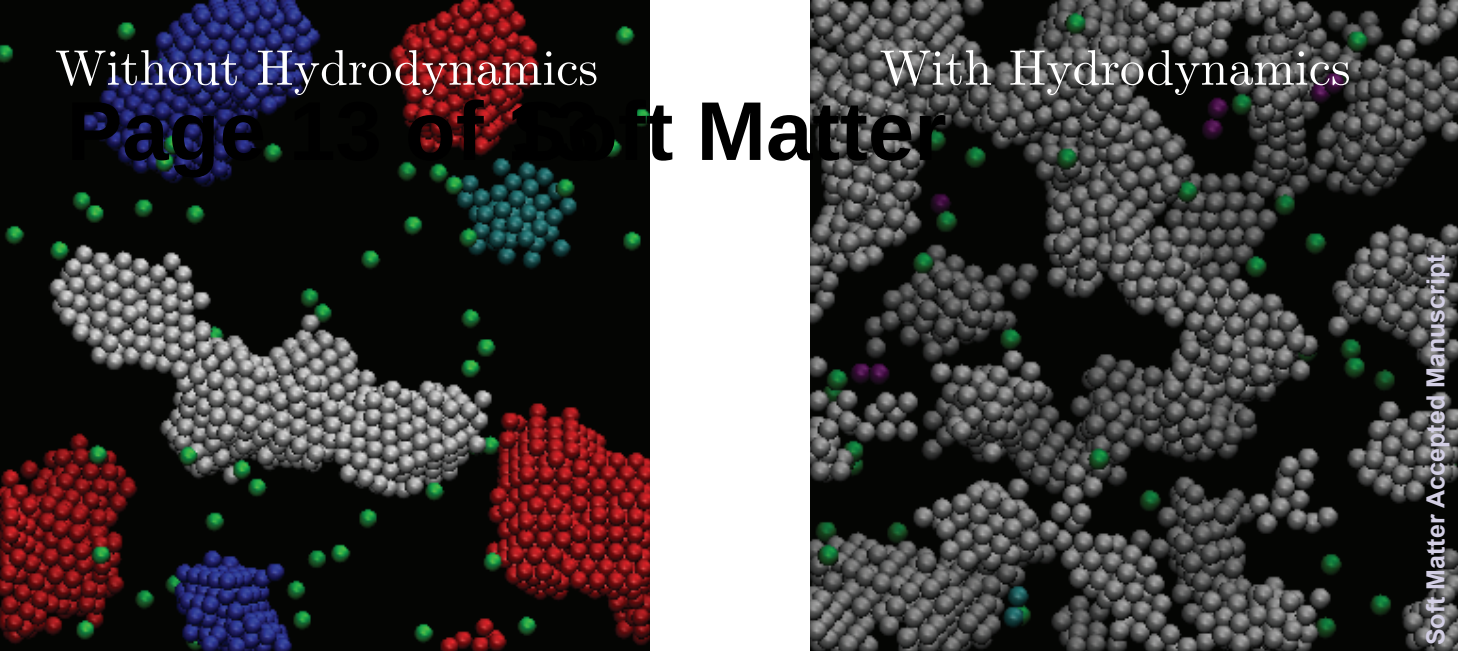

Simulations of attractive colloids with and without long-ranged hydrodynamic interactions indicate gelation boundary is sensitive to hydrodynamic flow.